Title

Fundus Autofluorescence in the Abca4−/− Mouse Model of Stargardt Disease—Correlation With Accumulation of A2E, Retinal Function, and HistologyFundus Autofluorescence in the Abca4 −/− Mouse

Journal

Investigative Ophthalmology & Visual Science, 54(8)

ISSN

0146-0404

Authors

Issa, Peter Charbel
Barnard, Alun R
Singh, Mandeep S
et al.

Publication Date

2013-08-19

DOI

10.1167/iovs.13-11688

Peer reviewed

Fundus Autofluorescence in the *Abca4*$^{-/-}$ Mouse Model of Stargardt Disease—Correlation With Accumulation of A2E, Retinal Function, and Histology

Peter Charbel Issa,[1,2] Alun R. Barnard,[1] Mandeep S. Singh,[1] Emma Carter,[1] Zhichun Jiang,[3] Roxana A. Radu,[3] Ulrich Schraermeyer,[4] and Robert E. MacLaren[1,5]

[1]Oxford Eye Hospital and Nuffield Laboratory of Ophthalmology, University of Oxford, Oxford, United Kingdom
[2]Department of Ophthalmology, University of Bonn, Bonn, Germany
[3]Jules Stein Eye Institute, Department of Ophthalmology, University of California at Los Angeles School of Medicine, Los Angeles, California
[4]University Eye Hospital, University of Tübingen, Tübingen, Germany
[5]Moorfields Eye Hospital and University College London Institute of Ophthalmology Biomedical Research Centre, London, United Kingdom

Correspondence: Peter Charbel Issa, Nuffield Laboratory of Ophthalmology, University of Oxford, John Radcliffe Hospital, OX3 9DU, UK; enquiries@eye.ox.ac.uk.
Robert E. MacLaren, Nuffield Laboratory of Ophthalmology, University of Oxford, John Radcliffe Hospital, OX3 9DU, UK; enquiries@eye.ox.ac.uk.

Submitted: January 18, 2013
Accepted: June 2, 2013

Citation: Charbel Issa P, Barnard AR, Singh MS, et al. Fundus autofluorescence in the *Abca4*$^{-/-}$ mouse model of Stargardt disease—correlation with accumulation of A2E, retinal function, and histology. *Invest Ophthalmol Vis Sci.* 2013;54:5602–5612. DOI: 10.1167/iovs.13-11688

Purpose. To investigate fundus autofluorescence (AF) characteristics in the *Abca4*$^{-/-}$ mouse, an animal model for AMD and Stargardt disease, and to correlate findings with functional, structural, and biochemical assessments.

Methods. Blue (488 nm) and near-infrared (790 nm) fundus AF images were quantitatively and qualitatively analyzed in pigmented *Abca4*$^{-/-}$ mice and wild type (WT) controls in vivo. Functional, structural, and biochemical assessments included electroretinography (ERG), light and electron microscopic analysis, and A2E quantification. All assessments were performed across age groups.

Results. In *Abca4*$^{-/-}$ mice, lipofuscin-related 488 nm AF increased early in life with a ceiling effect after 6 months. This increase was first paralleled by an accumulation of typical lipofuscin granules in the retinal pigment epithelium (RPE). Later, lipofuscin and melanin granules decreased in number, whereas melanolipofuscin granules increased. This increase in melanolipofuscin granules paralleled an increase in melanin-related 790 nm AF. Old *Abca4*$^{-/-}$ mice revealed a flecked fundus AF pattern at both excitation wavelengths. The amount of A2E, a major lipofuscin component, increased 10- to 12-fold in 6- to 9-month-old *Abca4*$^{-/-}$ mice compared with controls, while 488 nm AF intensity only increased 2-fold. Despite pronounced lipofuscin accumulation in the RPE of *Abca4*$^{-/-}$ mice, ERG and histology showed a slow age-related thinning of the photoreceptor layer similar to WT controls up to 12 months.

Conclusions. Fundus AF can be used to monitor lipofuscin accumulation and melanin-related changes in vivo in mouse models of retinal disease. High RPE lipofuscin may not adversely affect retinal structure or function over prolonged time intervals, and melanin-related changes (melanolipofuscin formation) may occur before the decline in retinal function.

Keywords: fundus autofluorescence, mouse model, *Abca4*, A2E

Mutations in the gene coding for the ATP-binding cassette A4 (ABCA4) transmembrane transporter cause autosomal recessive Stargardt disease, cone–rod dystrophy or retinitis pigmentosa.[1–5] Mutations in *ABCA4* are among the most common causes for inherited retinal dystrophies and may, in addition, modify the phenotype of other genetic and/or multifactorial retinal diseases, including AMD.[5–7]

Stargardt disease[8] is the phenotype most commonly caused by *ABCA4* mutations. A hallmark of the disease is an increased fundus autofluorescence (AF) exhibiting the fluorescence characteristics of lipofuscin in the retinal pigment epithelium (RPE).[9,10] Later, atrophy of the central retina develops, which spreads centrifugally over time.[11]

Based on findings in *Abca4*$^{-/-}$ mice, the lack of ABCA4 function results in marked accumulation of the bisretinoid N-retinylidene-N-retinylethanolamine (A2E) in the RPE.[12] A2E is a major component of RPE lipofuscin and appears to have a role in retinal disease pathophysiology. This includes its potential to increase blue light cytotoxicity,[13,14] induce lysosomal dysfunction,[15,16] and activate complement.[17] Increased RPE lipofuscin has been shown in postmortem specimens of *Abca4*$^{-/-}$ mice.[12,18–20] However, it is not known if this increase in lipofuscin/A2E levels is indeed correlated with increased fundus AF measured in vivo in *Abca4*$^{-/-}$ mice.

We recently showed the feasibility, reproducibility, and utility of standardized qualitative and quantitative fundus AF assessment in mice.[21] Being able to monitor A2E/lipofuscin accumulation using noninvasive fundus AF imaging would allow longitudinal in vivo assessment when evaluating potential treatments for Stargardt disease and other potentially lipofuscin-related retinopathies such as AMD. Moreover, studying this clinically meaningful imaging modality in the *Abca4*$^{-/-}$ mouse

along with further structural, biochemical, and functional parameters may have implications for interpreting the human retinal disease phenotype and natural history.

The aim of this study was to investigate quantitative and qualitative fundus AF characteristics in *Abca4*$^{-/-}$ mice at various ages compared with age-matched wild type (WT) controls. In addition to conventional fundus AF with short wavelength excitation (488 nm light), near-infrared (NIR) excitation (790 nm light) was also used. Results were correlated with tissue A2E levels, histologic findings, and retinal function using electroretinography (ERG).

Methods

Mice

Pigmented *Abca4*$^{-/-}$ mice (129S4/SvJae-*Abca*^{4tm1Gbt})[12] were provided by Gabriel Travis (David Geffen School of Medicine, University of California, Los Angeles, CA) and bred in the Biomedical Sciences division, University of Oxford. Pigmented WT control mice (129S2/SvHsd) were purchased from Harlan Laboratories (Hillcrest, UK). All experiments were conducted in female mice. The animals were kept in a 12 hour light (<100 lux)/dark cycle, with food and water available ad libitum. All animal breeding and experimental procedures were performed under approval of local and national ethical and legal authorities, and were conducted in compliance with the ARVO Statement for the Use of Animals in Ophthalmic and Vision Research. *Abca4*$^{-/-}$ and WT mice were homozygous for the (Leu450) allele of *Rpe65* (Supplementary Fig. S1).

Fundus Autofluorescence Imaging

Mouse fundus AF imaging was performed using a confocal scanning laser ophthalmoscope (cSLO; SpectralisHRA, Heidelberg Engineering, Heidelberg, Germany), according to a previously described standardized protocol.[21] Fluorescence was excited using a 488 nm argon laser or a 790 nm diode laser and emission was recorded at 500 to 700 or greater than 810 nm, respectively.

Animals were anesthetized by intraperitoneal injection of 1 mg/kg medetomidine (Dormitor 1 mg/mL; Pfizer, Sandwich, UK) and 60 mg/kg ketamine (Ketaset 100 mg/mL; Fort Dodge, Southampton, UK), and pupils fully dilated with tropicamide eye drops (Mydriaticum 1%; Bausch & Lomb, Kingston-Upon-Thames, UK) and phenylephrine eye drops (phenylephrine hydrochloride 2.5%, Bausch & Lomb). A custom made contact lens was placed on the cornea with hypromellose eye drops (Hypromellose eye drops BPC 0.3%; Matindale Pharmaceuticals, Romford, UK) as viscous coupling fluid. For image acquisition, the mouse was positioned on a platform mounted on the chin rest of the cSLO device. Only one eye per mouse was recorded.

All images were recorded using the 55° lens (Heidelberg Engineering) of the Spectralis HRA. The NIR reflectance image (820 nm diode laser) was used to align the fundus camera relative to the pupil and to focus on the confocal plane of highest reflectivity in the outer retina.[21] Images were recorded using the "automatic real time" (ART) mode, which is able to track ocular movement (e.g., due to respiration) based on high contrast landmarks. The ART mode allows averaging of up to 100 consecutive images in real time, resulting in an improved signal-to-noise ratio.

Image Analysis

For quantitative analysis of fundus AF, the mean grey level on mouse fundus AF images (acquired with standardized signal detector sensitivity, unprocessed, 1536 × 1536 pixels) was measured within a ring shaped area between 250 and 450 pixel radii from the optic disc center (Supplementary Fig. S2) using ImageJ software (Version 1.43, National Institutes of Health, Bethesda, MD; http://rsb.info.nih.gov/ij). The "electronic zero" was subtracted from each measured grey value to obtain the corrected grey level (cGL), which was used for all calculations.

Electroretinography

Animals were dark adapted for at least 6 hours before ERG responses were recorded from one eye. The other eye remained undilated and was protected by a contact lens to facilitate subsequent cSLO imaging. A DTL-type silver-coated nylon thread active electrode (DTL Plus Electrode; Diagnosys LLC, Cambridge, UK) was modified to include a custom-made contact lens of clear Aclar film (Honeywell International, Inc., supplied by Agar Scientific, Stansted, UK). This was positioned concentrically on the cornea using hypromellose eye drops (1% methylcellulose solution) for coupling. Platinum needles in the scruff and at the base of the tail served as reference and ground electrodes, respectively. Signals were differentially amplified and digitized at a rate of 5 kHz using an Espion E2 system (Diagnosys LLC, Cambridge, UK). The amplitude and latency of major ERG components were measured with the Espion software (Diagnosys LLC) using automated and manual methods. Brief (4 ms) single flash stimuli were delivered in a Ganzfeld dome. Animals were placed on a heated platform, maintained at 38°C using a circulating pump-water bath. All recordings were made in a custom-made light-tight Faraday cage.

For dark-adapted testing, responses were elicited by brief flashes of white light on a dark background. Stimulus intensity was increased across an approximately 5 log unit range (Supplementary Table S1). For light-adapted testing, animals were preexposed to steady full-field white background illumination (30 cd/m^2) for 10 minutes. The recovery of dark-adapted function was measured after a 30 second exposure to 1000-lux white light. For this latter experiment, *Abca4*$^{-/-}$ mice were crossed with WT mice and the heterozygote progeny intercrossed to obtain littermate homozygous *Abca4*$^{-/-}$ and WT mice. Further details of the ERG protocols are provided in Supplementary Tables S1 and S2.

In single flash ERGs, the b-wave amplitude (from a-wave trough to b-wave peak) was measured for all ERGs, whereas the a-wave amplitude (from baseline to a-wave trough) was measured only when recognizable as a distinct component (stimulus intensities $\geq$ 0.1 cd.s/m^2). Both amplitudes were measured in unfiltered recordings. Amplitudes of flicker ERGs were measured in recordings with 0 to 100 Hz bandpass and 50 Hz notch filters applied.

Preparation and Embedding for Light and Electron Microscopy

After enucleation, the eyes were cleaned of orbital tissue and, after removal of the cornea, were fixed overnight at 4°C in 2% glutaraldehyde in 0.1 M cacodylate buffer (pH 7.4) containing 100 mM sucrose. After washing with cacodylate buffer, areas of interest in flat mount preparations were excised and post-fixed with 1% osmium tetroxide in 0.1 M cacodylate buffer at room temperature for 1 hour. Dehydration was then started by a series of incubations in 30%, 50%, and 70% ethanol. The samples were stained with saturated uranyl acetate. Dehydration was continued by incubations in 70%, 80%, 95% ethanol, absolute ethanol, and propylene oxide. The samples were then embedded in Epon (SPI-Pon812 Epoxy Embedding Kit; SPI

Investigative Ophthalmology & Visual Science

supplies, West Chester, PA). For light and fluorescence microscopy, staining with osmium and uranylacetate was omitted.

Electron Microscopy and Pigment Granule Quantification

Ultrathin Epon sections (70 nm) from WT control eyes and *Abca4*$^{-/-}$ eyes were post stained with lead citrate and investigated under a transmission electron microscope (TEM; Model 902 A; Carl Zeiss, Oberkochen, Germany). For statistical analysis, the areas occupied by different types of pigment granules were quantified in 5 to 8 micrographs from each group. As lipofuscin is somewhat unusual in *Abca4*$^{-/-}$ mice, the morphologic definition we used in this study of the RPE was as follows: lipofuscin in *Abca4*$^{-/-}$ mice is a type of intracellular granule, which appears in the electron microscope as a membrane bound body with heterogeneous staining and very variable shape generally darker than the cytosol. Melanin granules are easily and reliably distinguished from lipofuscin in the electron microscope, in that melanosomes are uniformly electron dense (black), are not fused with other organelles and appear spindle shaped, ovoid, or round. Melanosomes that are fused with lipofuscin are considered as melanolipofuscin and were included in the combined category of lipofuscin and melanolipofuscin. For lipofuscin and melanolipofuscin quantification, image analysis software (iTEM; Olympus Soft Imaging Solutions, Münster, Germany) was used. For each image, the total area of RPE cytoplasm was determined. Nuclei were not included in this measurement. Apical microvilli and extracellular space in the region of the basal infoldings were also excluded. The included area totaled from approximately 50 to 100 μm^2 per image. The area fraction of lipofuscin/melanolipofuscin is expressed as area in squared micrometers occupied by lipofuscin per 1000 μm^2 RPE cytoplasm.

Fluorescence Microscopy

Autofluorescent lipofuscin and melanolipofuscin granules were photographed in semi-thin sections using a fluorescence microscope (Zeiss Axioplan 2; Carl Zeiss, Jena, Germany; excitation 370/36 nm, emission 575/15 nm, 40× objective) connected to a computer equipped with a CCD camera (Orca-ER; Hamamatsu Photonics, Hamamatsu, Japan). Since the granules could not clearly be separated from each other and lipofuscin cannot be differentiated from melanolipofuscin, the quantification of lipofuscin granules was only performed using electron microscopy.

Outer Nuclear Layer Count

Eyes were dissected in 4% paraformaldehyde (Thermo Fisher, Loughborough, UK) in PBS. After fixation for 30 to 45 minutes, the eyecups were transferred to 30% sucrose for cryoprotection and kept at 4°C overnight. Eyecups were embedded in optimal cutting temperature (OCT) compound (Tissue-Tek, Sakura Finetek, The Netherlands) and frozen on dry ice. Serial 16-μm thick cryosections were affixed to poly-L-lysine–coated glass slides (Polysine; Thermo Scientific, Loughborough, UK), air dried and then stored at −20°C until further histologic processing. Outer nuclear layer (ONL) count was performed after nuclear staining using Hoechst 33342 (Invitrogen Ltd., Paisley, UK) 1:5000 at three eccentricities, 500 and 1000 μm from the optic disc center, and 500 μm from the ora serrata. Nuclei were counted manually within a box of fixed width (20 pixels ≈ 19.6 μm) placed over the ONL. To present data as number of nuclear layers, the total ONL nuclear count was divided by the number of nuclei along the width of the box. Per eye, results from three sections and both sides of the optic nerve head were averaged.

Quantification of A2E

For A2E quantification, the cornea and lens were removed in PBS. Dissected eye cups were immediately snap frozen and stored at −80°C until further processing. The detailed method of *bis*-retinoids extraction and analysis is described in the paper by Radu et al.[22]

Statistical Analysis

PRISM (Version 6.02; GraphPad Software, La Jolla, CA) was used for statistical analysis. Two-way ANOVA was performed to detect significant differences between *Abca4*$^{-/-}$ mice and WT controls, using strain and age as factors. The Holm-Sidak or Bonferroni method was applied in all instances to correct for multiple testing (e.g., in pairwise comparisons). The significance level was set at 0.05.

Results

Longitudinal Recordings of 488 and 790 nm Fundus AF Intensity

Repeated recordings in the same animals were performed between the ages of 1 and 9 months in *Abca4*$^{-/-}$ mice and WT controls to investigate the change in fundus AF levels over time. 488 and 790 nm fundus AF in *Abca4*$^{-/-}$ mice were similar to WT at 1 month (Figs. 1A, 1B). Thereafter, 488 nm fundus AF rose significantly faster in *Abca4*$^{-/-}$ mice compared with WT, leveling off at 6 months (Fig. 1A). Following a different time course, 790 nm AF in *Abca4*$^{-/-}$ mice increased relative to WT only after 3 months of age (Fig. 1B). 488 nm fundus AF levels in all 9-week-old or older *Abca4*$^{-/-}$ mice studied were higher than the 95% confidence interval (CI) of WT measurements. The same applied for 790 nm AF in *Abca4*$^{-/-}$ mice aged 6 and 9 months.

Pupil size, which has a major impact on measured fundus AF in mice,[21] significantly increased with age in both strains to a similar degree (Supplementary Fig. S3). Thus, differences in pupil size would not explain the differences between strains.

Fundus AF levels in *Abca4*$^{-/-}$ mice were normalized to that in age-matched WTs to control for possible age-related confounders including pupil size, and, thus, to allow a better estimation of the effect of *Abca4* deficiency on AF levels over time (Fig. 1C). 488 nm AF rose from 1.2× that of WT at 1 month, to 2× by 3 months, to a maximum of approximately of 2.2×, thereafter showing a ceiling effect. 790 nm AF was 1× WT level in the first 3 months, increased to 1.7× from 3 to 6 months, and to 1.9× by 9 months.

Cross-Sectional Recordings of 488 and 790 nm Fundus AF

To investigate AF in aged animals naïve to any imaging that may have influenced A2E levels, separate cohorts of *Abca4*$^{-/-}$and WT control mice were assessed cross sectionally at 3, 6, 9, 12, and 18 months of age. Eyes of these animals were used to correlate fundus AF levels with postmortem A2E measurements and histology (see below). Quantitative fundus AF assessment in animals 12 months and older was hampered by suspected incident cataract in *Abca4*$^{-/-}$ and WT mice. AF levels in animals aged 3, 6, and 9 months from this independent cross-sectional cohort confirmed the findings of the longitudinal assessment (Supplementary Table S3), and suggested that repeated cSLO imaging in the longitudinally observed animals did not

Investigative Ophthalmology & Visual Science

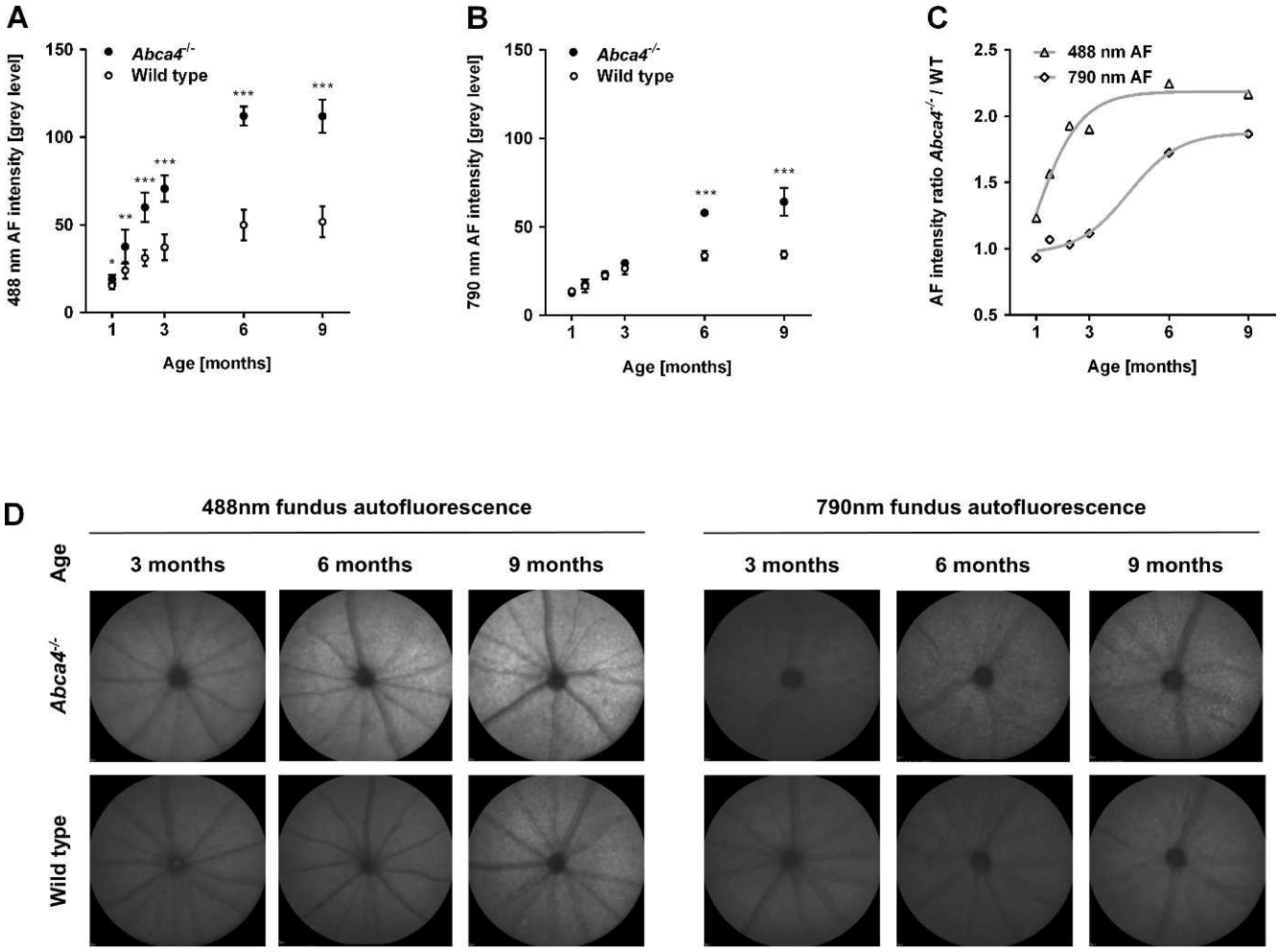

Figure 1. (**A–C**) Longitudinal measurements of fundus AF intensity in the *Abca4*$^{-/-}$ mouse ($n = 5$) and WT ($n = 8$) controls between 1 to 9 months of age. To distinguish lipofuscin- and melanin-related fundus AF, 488 (**A**) and 790 nm (**B**) wavelengths were used for excitation, respectively. Levels of fundus AF (mean ± SD) were significantly different between strains and between age groups ($P < 0.01$, two-way ANOVA) for 488 and 790 nm fundus AF. $^{*}P < 0.05$; $^{**}P < 0.01$; $^{***}P < 0.001$. (**C**) Using the ratio of mean fundus AF between *Abca4*$^{-/-}$ and WT mice controlled for age-related factors potentially affecting AF intensity measures. Curves were fitted to illustrate the time course of AF increase in *Abca4*$^{-/-}$ relative to WT at the two different excitation wavelengths. (**D**) Unprocessed representative recordings of fundus AF excited at 488 and 790 nm in *Abca4*$^{-/-}$ and WT control mice (cross-sectional cohort). Overall, the AF signal was higher with 488 nm compared with 790 nm excitation light. At 3, 6, and 9 months, 488 nm AF in *Abca4*$^{-/-}$ mice is higher than in WT, with a larger difference in older animals. 790 nm AF was only significantly different in 6 and 9 months old animals, where *Abca4*$^{-/-}$ mice show a higher AF level than controls.

significantly modify AF levels over time. Representative recordings with an age- and strain-dependent increase of fundus AF intensity are shown in Figure 1D.

Qualitatively, flecks of increased or decreased 488 nm AF were obvious in 6-month-old *Abca4*$^{-/-}$ mice (Fig. 2A), whereas in WT these appeared later at 9 months and were noticeably less distinct. On 790 nm AF, a fleck pattern was consistently observed in *Abca4*$^{-/-}$ mice 6 months and older. Flecks on 790 nm AF were not seen in WT controls up to the age of 18 months.

Large areas of geographic atrophy, as typically observed in patients with Stargardt disease, were not observed. However, in *Abca4*$^{-/-}$ mice 12 months and older, there were spots of decreased AF. Such loss of fluorophores may suggest focal damage and/or incident atrophy of the RPE. Overall, this was observed more frequently in 790 nm AF, sometimes in presence of near-normal 488 nm AF pattern (Figs. 2B, 2C). In a few eyes the opposite pattern occurred (i.e., that a reduced 488 nm AF was more obvious alongside near-normal 790 nm AF [Fig. 2D]).

Comparison of Fundus AF Recordings and A2E Measurements

A2E is regarded as a major fluorophore of lipofuscin at the ocular fundus. Therefore, we assessed if A2E levels in *Abca4*$^{-/-}$ and WT control mice increased in parallel with 488 nm AF levels (cross-sectional data set). AF ratios between *Abca4*$^{-/-}$ and WT mice confirmed results from the longitudinal data set. 488 nm AF levels in *Abca4*$^{-/-}$ mice were approximately 1.8-fold higher than controls at 3 months and approximately 2-fold at 6 and 9 months (Fig. 3A). In contrast, A2E levels in 3-month-old *Abca4*$^{-/-}$ mice were 8 times higher than controls and increased to approximately 12-fold at 9 months (Fig. 3B).

Electroretinography

In *Abca4*$^{-/-}$ and WT control mice, scotopic a-wave and b-wave amplitudes depended on age and stimulus intensity (Supplementary Fig. S4, Figs. 4A, 4B; two-way ANOVA, all $P < 0.001$). a- and b-wave amplitudes depended on stimulus intensity in all age groups, but only in 18-month-old animals were affected by

Investigative Ophthalmology & Visual Science

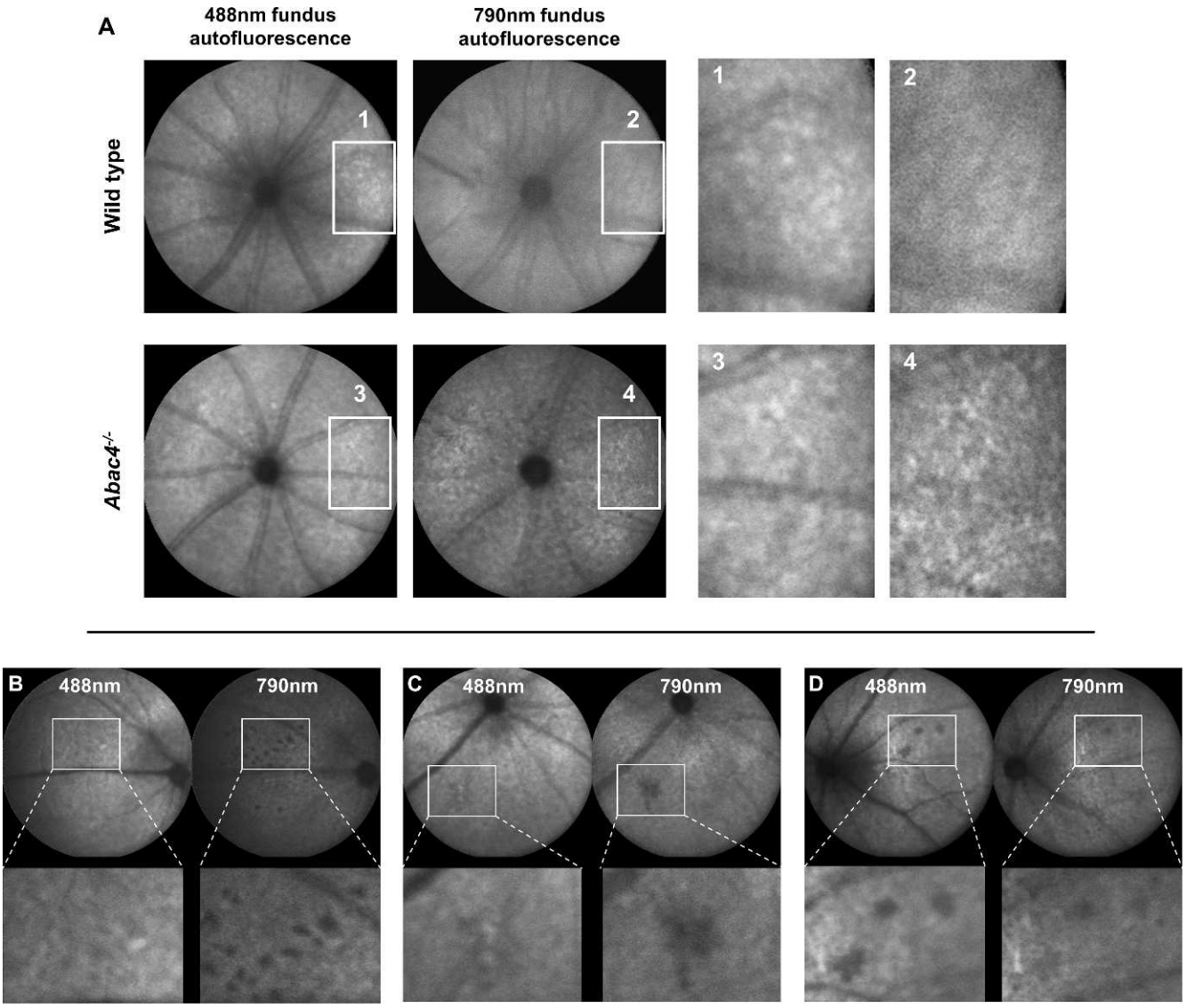

Figure 2. (**A**) Representative AF fleck patterns in a 12-month-old *Abca4*$^{-/-}$ mouse and an age-matched control (images processed for contrast). Flecks on 488 nm AF images were visible in both mice but were more pronounced in the *Abca4*$^{-/-}$ mouse. On 790 nm AF, a fleck pattern was only visible in the *Abca4*$^{-/-}$ mouse, but not in the WT control. (**B**–**D**) Dark areas on fundus AF imaging suggesting focal damage of the RPE in aged *Abca4*$^{-/-}$mice. (**B**, **C**) 488 nm fundus AF (*left*) in a 12- (**B**) and 18- (**C**) month-old mouse showing fleck-like increased AF and faint spots of reduced AF. The latter are also hypofluorescent on the 790 nm AF image (*right*). (**D**) Rarely, spots of markedly reduced AF were more obvious on 488 nm AF images. These lesions were not seen in similarly aged WT mice.

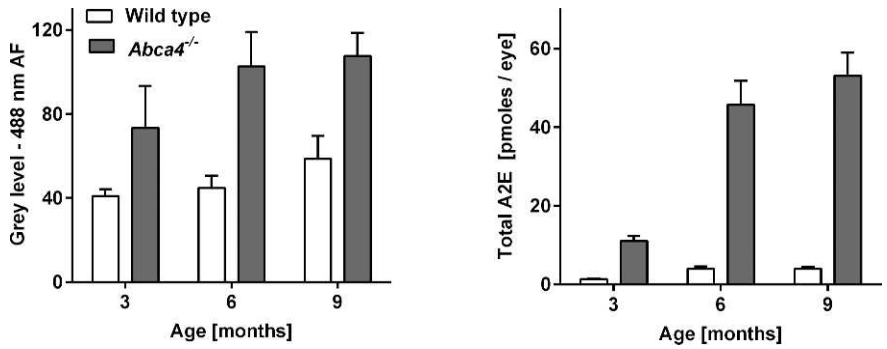

Figure 3. Difference of mean ± SD fundus AF intensity and A2E-levels between *Abca4*$^{-/-}$ and WT control mice aged 3, 6, and 9 months. While fundus AF intensity approximately doubles in *Abca4*$^{-/-}$ mice compared with controls (*left*), A2E levels are 10 and 12 times higher in *Abca4*$^{-/-}$ mice aged 6 and 9 months, respectively (*right*).

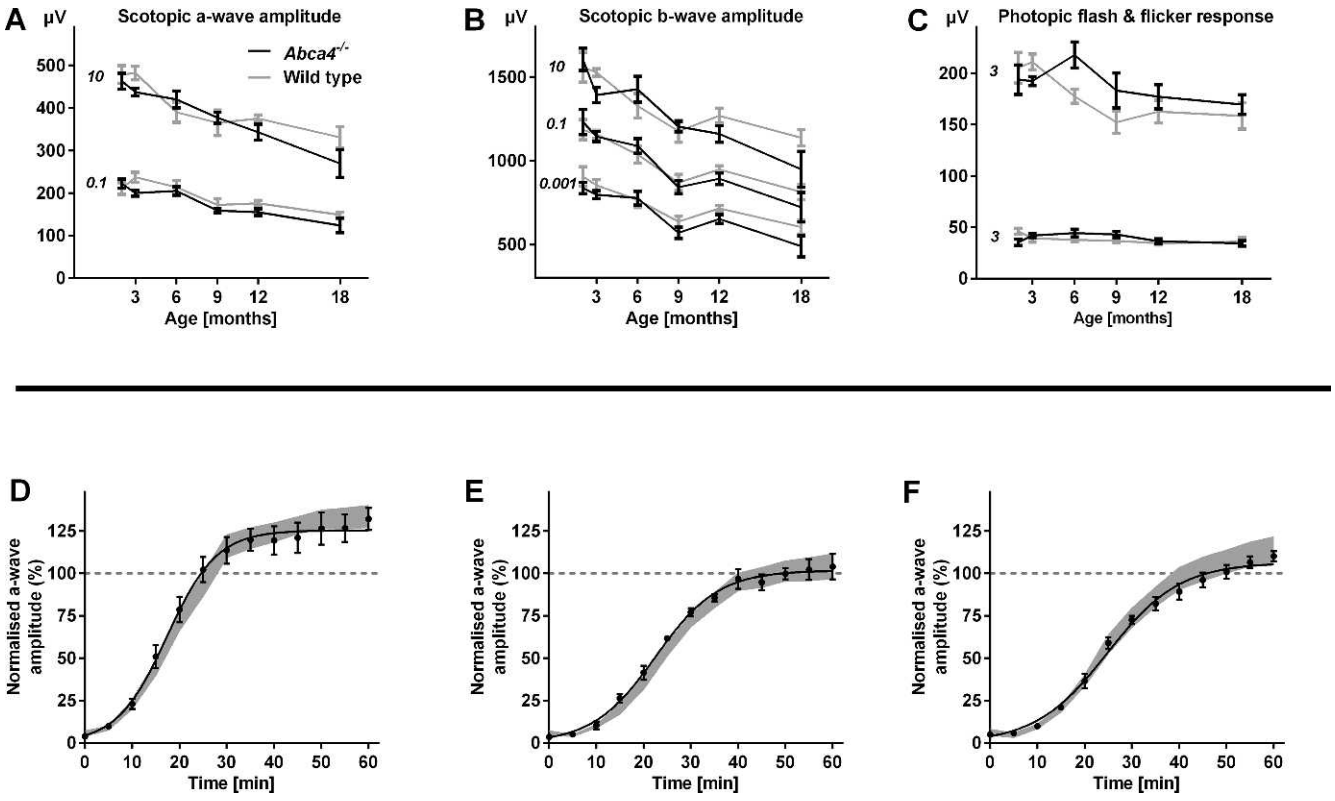

Figure 4. Functional testing by means of electroretinography in *Abca4*$^{-/-}$ and WT control mice. (**A–C**) Mean scotopic and photopic amplitudes ± SEM across all tested ages for representative flash intensities (for full range of mean traces see Supplementary Fig. S4). Numbers in italics indicate flash intensity in cd/m^2. The only significant difference between *Abca4*$^{-/-}$ mice and WT controls was observed in the scotopic testing of 18-month-old animals. *n* equals 5 to 8 in each group, except *n* equals 4 for 18-month-old WTs. (**D–F**) Kinetics of dark adaptation in *Abca4*$^{-/-}$ compared with WT control mice ($n = 5$–7 in each group) aged 1 (**D**), 4 (**E**), and 8 (**F**) months. The mean (±SEM) scotopic a-wave amplitude relative to baseline before a photobleach is shown. The *grey area* represents the mean ± 2SDs of the dark adaptation kinetics in WT mice. Recovery after photobleach was faster in 1-month-old compared with 4- and 8-month-old animals. Dark adaptation kinetics were similar in *Abca4*$^{-/-}$ and WT control mice.

genotype (two-way ANOVA, $P < 0.05$). Scotopic and photopic flicker ERG as well as photopic flash ERG were no different in *Abca4*$^{-/-}$ compared with WT mice (Supplementary Fig. S4, Fig. 4C).

The mean EC50 (as a sensitivity parameter) and mean hill slope (as a parameter for the dynamic range) on curve-fitted a-wave recordings in *Abca4*$^{-/-}$ mice were similar to WT mice, and did not vary with age (two-way ANOVA) at all intensities. Mean V_{max} (the maximum amplitude) varied with age ($P < 0.001$) but not genotype (two-way ANOVA). Bonferroni-corrected post hoc analysis revealed significant differences between animals aged 18 and 2 ($P < 0.001$), 3 ($P < 0.001$), and 6 ($P < 0.01$) months, as well as between mice aged 2 and 9 ($P < 0.05$), and 12 ($P < 0.001$) months.

Based on previous reports of an inhibitory effect of A2E on RPE65,[23] a key enzyme in the visual cycle, we hypothesized that dark adaptation after a photobleach as a functional measure for visual cycle efficiency would be slowed down with age (thus, significantly increased A2E-levels) in the *Abca4*$^{-/-}$ mouse compared with age-matched WT controls. Baseline a-wave amplitudes before the photobleach decreased with age, but were not different between strains (Supplementary Fig. S5), recapitulating the above results in a separate set of animals. Dark adaptation after a photobleach was slower in 4- and 8-month-old *Abca4*$^{-/-}$ mice than at age 1 month (Supplementary Fig. S5, Figs. 4D–F). This age effect was similar in WT mice.

Bright Light and Fluorescence Microscopy

In line with the functional ERG data, quantification of the photoreceptor layer thickness revealed loss of photoreceptors with age in *Abca4*$^{-/-}$ mice similar to WT controls up to 18 months (Supplementary Fig. S6). Semithin sections (Fig. 5A) qualitatively illustrate the similarity between retinas of *Abca4*$^{-/-}$ and WT mice even in 18-month-old animals. In contrast, the RPE of *Abca4*$^{-/-}$ mice showed marked structural differences compared with WT controls, with bright dots representing extensively accumulated lipofuscin granules (arrowhead in Fig. 5A). Also vacuolisation of RPE cells was observed focally in 18-month-old *Abca4*$^{-/-}$ mice (Supplementary Fig. S7). Under fluorescent light, lipofuscin was virtually absent in 3-month-old WT mice and increased little in animals aged 12 and 18 months (Fig. 5B). In contrast, fluorescent granules accumulated extensively with age in *Abca4*$^{-/-}$ mice.

Ultrastructural Observations in the TEM

The retina, RPE, and choroid tissues were examined to determine ultrastructural differences in *Abca4*$^{-/-}$ mice and WT controls. Prominent differences were only detected in the RPE. In young *Abca4*$^{-/-}$ mice, electron-opaque homogeneous granules as shown in Figure 6A were frequent, but significantly reduced in number in 12-month-old *Abca4*$^{-/-}$ mice. These granules had the typical appearance that has been described in aged human or monkey RPE and were nearly completely absent in WT mice. With increasing age in *Abca4*$^{-/-}$ mice,

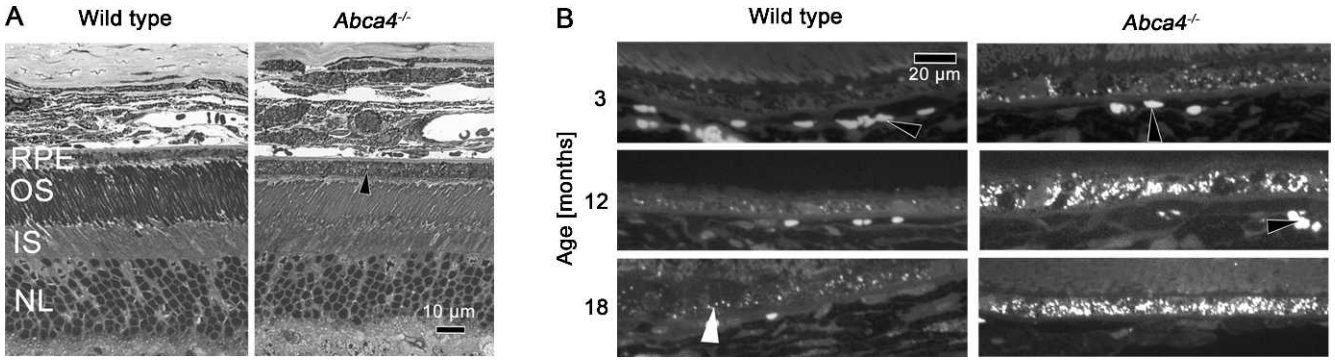

Figure 5. (**A**) Bright light microscopy of semithin sections of eyes from *Abca4*$^{-/-}$ and WT mice. In the RPE of 18-month-old *Abca4*$^{-/-}$mice bright dots (*arrowhead*) representing lipofuscin are detected, but are lacking in the age-matched WT control. Retinal morphology is otherwise similar. (**B**) Under fluorescent light, lipofuscin AF is virtually absent in WT mice at age 3 months and increased only little at 12 and 18 months. In contrast a strong accumulation of fluorescent granules with age occurred in *Abca4*$^{-/-}$ mice. Individual lipofuscin granules are indicated by a *white arrowhead*. Red blood cells also are somewhat autofluorescent (*black arrowheads*). OS, photoreceptor outer segments; IS, photoreceptor inner segments; NL, photoreceptor nuclear layer.

unusual material accumulated in the cytoplasm of RPE cells (Fig. 6), irregular in shape and electron dense. This type of organelle was nearly absent from WT mice. Although it is possible that these organelles are similar to the typical membrane bound lipofuscin granule, membranes were difficult to detect. The latter organelles showed a tendency to fuse with each other and occasionally with melanosomes (Fig. 6B). Eighteen-month-old mice of both groups contained electron opaque material between Bruch's membrane and basal infoldings (asterisks in Fig. 6A).

Quantification of Lipofuscin Granules by Electron Microscopy

The total areas (μm^2) occupied by lipofuscin and melanolipofuscin per 1000 μm^2 sectioned RPE cytoplasm was significantly higher in *Abca4*$^{-/-}$ mice at 12 and 18 months (53.4 $\pm$ 39.2 μm^2 and 115.6 $\pm$ 18.8 μm^2) compared with age-matched WT mice (2.2 $\pm$ 3.9 μm^2 and 0.5 $\pm$ 1.1 μm^2; Fig. 6C). This increase was statistically significant at 12 and 18 months of age ($P < 0.001$, Dunnett's test) but not at 3 months. The classical lipofuscin granules shown in Figure 6A occupied 16.1 $\pm$ 6.9 μm^2 in 3-month- and 5.7 $\pm$ 6.6 μm^2 in 12-month-old *Abca4*$^{-/-}$ mice ($P < 0.02$). They were virtually absent in 18-month-old *Abca4*$^{-/-}$ mice.

Discussion

488 and 790 nm Fundus AF: Its Relation to A2E Accumulation and Subcellular RPE Alterations

Quantitative analysis of AF intensity was performed in animals aged up to 9 months, when *Abca4*$^{-/-}$ mice were not different from WT controls in function and photoreceptor count, and without media opacity that could influence AF measurement. Because fundus AF quantification in mice is influenced by various factors that change with age, such as pupil width, eye size, and optical magnification,[21] AF measures in *Abca4*$^{-/-}$ mice were normalized to WT controls. This should control for age-related changes in knock-out and control mouse strains.

The ratio of 488 nm AF measurements between *Abca4*$^{-/-}$ and WT mice increased steeply within the first 3 months of life to approximately two, followed by a ceiling effect with only a minor further increase until age 9 months. These values are similar to those previously reported in patients with Stargardt disease compared with healthy controls.[24,25] Although the ratio of A2E levels between *Abca4*$^{-/-}$ and WT mice changed with a similar time course, its increase was considerably higher. One hypothesis to explain this discrepancy (assuming *Abca4*$^{-/-}$ mice had *bis*-retinoid and AF levels similar to WT mice at birth) would be that a substantial fraction of the 488-nm fundus AF signal in WT mice derives from fluorophores other than A2E and related *bis*-retinoids that do not vary considerably between WT and *Abca4*$^{-/-}$ mice (e.g., connective tissue flavoproteins, retinoids that do not depend on functional ABCA4; Fig. 7). A large increase in A2E content would then be necessary before relevant changes of 488 nm AF may be detected. Thus, increased 488 nm fundus AF levels parallel the accumulation of A2E in the RPE of *Abca4*$^{-/-}$ mice, but may not quantitatively represent its accumulation in direct proportion. Such "incongruence" was also reported based on post mortem experiments by Boyer et al. who found a lack of correspondence in the rates of increase between lipofuscin-related AF in eyecups and quantification of A2E.[26] Similar to our data, AF and A2E-levels in eyes from aged *Abca4*$^{-/-}$ mice (background strain: 129Sv) compared with WT controls were approximately 2- and 10-fold higher, respectively.[26] The same authors also reported incongruence between lipofuscin-related AF and A2E levels across different WT mouse strains: while eyecup AF intensity in the C57BL/6 strain was higher compared with the 129Sv strain, A2E-levels were lower. Such differences of AF intensity based on genetic background were also observed in our experiments (not reported in detail; Supplementary Fig. S8) and may be of interest when interpreting quantitative AF measures in humans.[27] Boyer et al.[26] also challenged the current hypothesis on the function of ABCA4 by providing evidence that light exposure and thus all-*trans*-retinal formation is not necessary for accumulation of A2E- and lipofuscin in the RPE. Assessment of AF intensity in vivo in dark-reared animals was not performed in our study, but would complement those findings.

An additional explanation for the faster increase of A2E-levels compared with AF levels would be an interaction between lipofuscin-accumulation and fundus AF intensity. Lipofuscin located in the apical RPE cell compartment may absorb excitation light and, thus, reduce the contribution to the AF signal from more basally located lipofuscin.

Melanin-related 790-nm AF levels also revealed a pronounced but considerably later increase compared with 488 nm AF. The major fluorophore for NIR excitation and thus the origin of 790 nm AF at the ocular fundus appears to be melanin.[28] Oxidative stress on the RPE has been suggested to play a pathophysiologic role in a variety of retinal diseases, and

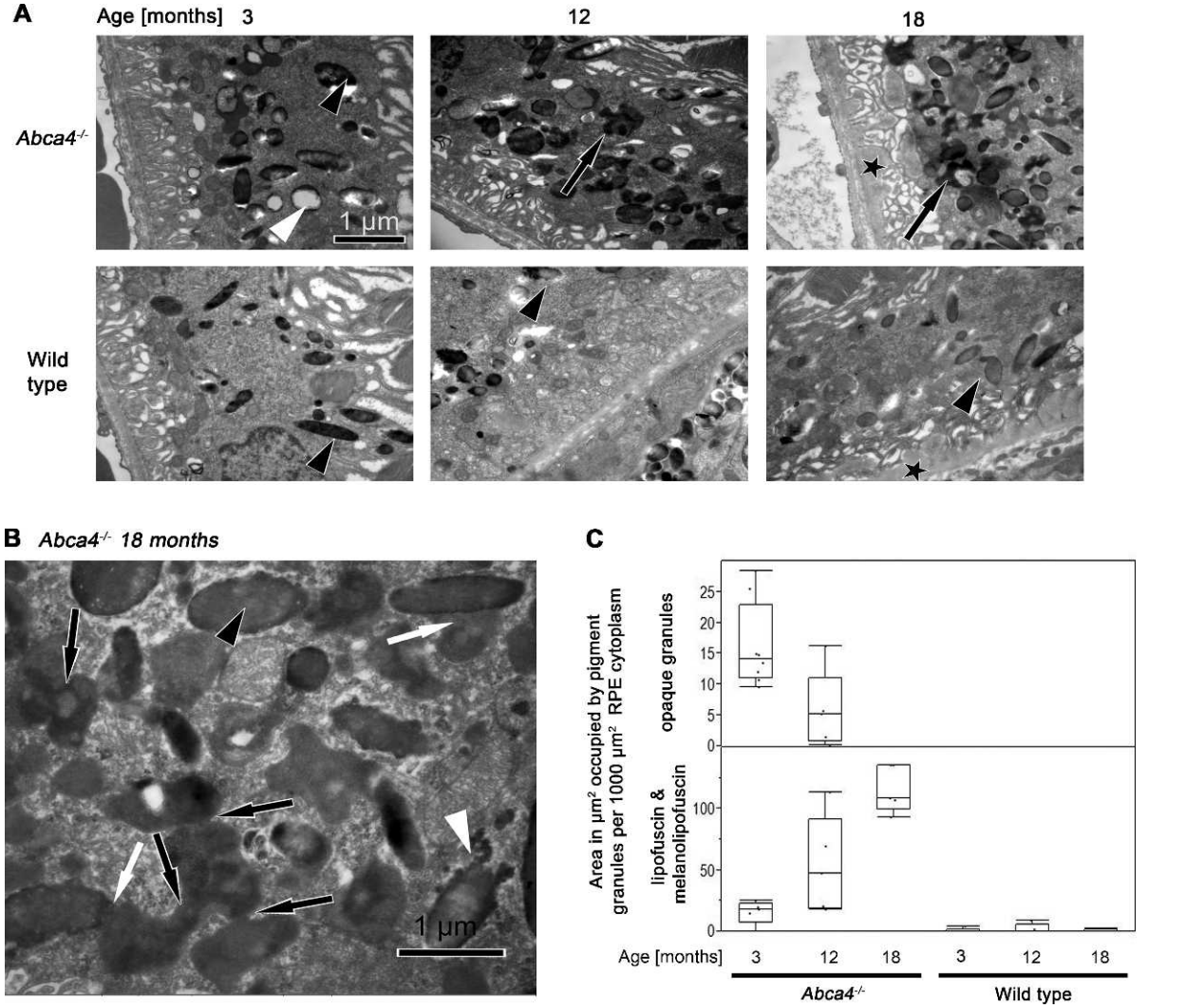

Figure 6. (**A**) TEM micrographs of RPE cells of from *Abca4*$^{-/-}$ and WT mice at ages 3, 12, and 18 months. In 3-month-old *Abca4*$^{-/-}$ mice electron-opaque homogeneous granules are labeled by a *white* and a melanosome by a *black arrowhead*. The granule labeled by the *white arrowhead* represents the more classical type of lipofuscin. With progression of age, unusual granules of irregular shape and electron density (*black arrows*) accumulate in the RPE cytoplasm of 12- and 18-month-old *Abca4*$^{-/-}$ mice. This type of organelle is nearly absent from WT mice. Melanosomes are indicated by *black arrowheads*. Eighteen-month-old mice of both groups contain electron opaque material (*asterisks*) between Bruch's membrane and basal infoldings. (**B**) TEM micrograph of the RPE from an 18-month-old *Abca4*$^{-/-}$ mouse at high magnification. With progression of age, unusual granules accumulated in the cytoplasm of RPE cells. A melanosome is marked by an *arrowhead* and Bruch's membrane by an *asterisk*. The material accumulated in the cytoplasm is irregular in shape and electron dense (*black arrows*). These granules appear to fuse with each other (*black arrows*) and with melanosomes (*white arrows*). The electron density of these confluent granules is occasionally as dense as in melanosomes (*black arrowhead*). A melanosome in a state of disintegration is indicated by a *white arrowhead* and were also present in WT mice. (**C**) Quantification of lipofuscin and melanolipofuscin granules by electron microscopy. The total areas (µm^2) occupied by lipofuscin and melanolipofuscin per 1000 µm^2 sectioned RPE cytoplasm increased significantly in *Abca4*$^{-/-}$ mice at 12 and 18 months compared with age-matched WTs. The area occupied by the classic (*opaque*) lipofuscin granules in *Abca4*$^{-/-}$ mice declined with age.

oxidation of melanin has been shown to increase its autofluorescence.[29,30] The observed time course of 790 nm AF could therefore be explained by increased oxidative stress in RPE cells after pronounced A2E accumulation. Based on electron microscopy findings, a significant increase in melanin-related AF due to an increase in melanin granules appears unlikely. However, melanin granules revealed marked morphologic alteration with a similar time course as the increase in 790 nm AF. Oxidative stress increases in RPE cells with increased lipofuscin load, possibly leading to melanin oxidation and formation of melanolipofuscin granules. Thus, altered AF properties of melanin (e.g., through oxidation or fusion with lipofuscin granules) appear to be the most likely explanation for the increased 790 nm AF. It is notable that in contrast to the results of this study, in albino *Abca4*$^{-/-}$ mice there is a progressive photoreceptor cell loss that is detectable at 8 months of age and worsens at 11 and 13 months.[31] Because melanin has an antioxidative capacity[32] the formation of melanolipofuscin as observed in the present study may reduce the formation of oxidative damage caused by lipofuscin alone.

No larger areas of RPE atrophy similar to those observed in Stargardt patients were observed in animals up to an age of 18 months. However, small patches of AF loss suggestive for RPE damage were observed in some *Abca4*$^{-/-}$ mice 9 months and older, but were never present in WT mice of similar age.

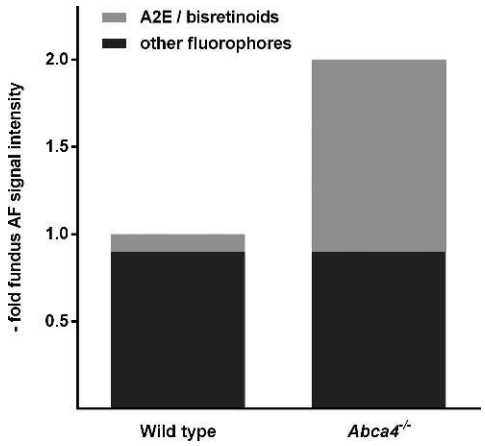

FIGURE 7. Model to explain the discrepancy between the approximate 2-fold higher fundus AF levels and approximate 10-fold higher A2E levels in *Abca4*$^{-/-}$ mice compared with WT controls. There may be only a low contribution of A2E and related bis-retinoids to fundus AF intensity in WT mice.

Besides RPE cell atrophy and/or a change in fluorophores, vacuolization within the RPE (Supplementary Fig. S7) might contribute to this finding. Loss of 790 nm AF often appeared to precede loss of 488 nm AF. Those findings suggest that high A2E levels may not be the direct cause of damage within the RPE, which appears to develop after an increase in melanin-related AF. If oxidation products of A2E are causing the changes in the melanin compartment and/or are cytotoxic, increased light exposure might lead to earlier development of the observed changes.

Functional Relevance of Increased Fundus AF Levels and A2E Accumulation

Despite the high levels of fundus AF and A2E in *Abca4*$^{-/-}$ mice early in life (i.e., in 2- to 3- month-old animals), no areas of atrophy similar to those observed in Stargardt patients were observed up to 18 months of age. Also, such high lipofuscin contents in the RPE remained without functionally relevant damage over prolonged time intervals, as shown by ERG testing. Thus, high A2E levels can be tolerated by RPE cells over prolonged time periods, and additional factors such as high oxidative stress or the macular anatomy appear to be necessary to develop RPE atrophy.

Notably, an increase in 790-nm AF intensity preceded functional differences between *Abca4*$^{-/-}$ and WT mice and occurred before the appearance of small atrophy-resembling spots on AF images. Thus, alterations in the melanosomal compartment, as revealed by 790-nm AF imaging, seem to precede structurally and functionally relevant changes in the RPE.

Assessment of dark adaptation revealed an effect of age in *Abca4*$^{-/-}$ and WT mice. This effect was similar between strains, suggesting that there is no relevant effect of the lack of ABCA4. Notably, the change in dark adaptation rate from 1 to 4 months of age was similar between strains despite the very steep increase of A2E and lipofuscin-related AF levels in *Abca4*$^{-/-}$ mice. This suggests that an inhibitory effect of A2E on RPE65 may not be an important contributor to delayed dark adaptation in vivo. It should be noted that protocols, background strains, assessed parameters, and analysis to describe the dark adaptation characteristics in *Abca4*$^{-/-}$ mice vary considerably in the literature,[12,33–36] which may be the reason heterogeneous and partly unreproducible results across studies. Our protocol assessing recovery of scotopic single flash amplitudes aimed at identifying differences in retinoid cycle kinetics after a photobleach. Although there might be a trend for a declining dark-adaptation rate in aged *Abca4*$^{-/-}$ compared with WT controls (Fig. 4F), the difference of this parameter might not be substantial and robust enough to assess treatment effects in preclinical studies. Paired-flash ERG analysis and similar protocols may identify reduced photoreceptor sensitivity states, for which the protocol used in this study would not be suitable.

Comparison With Human Disease

Cideciyan et al. have proposed six stages of the human disease sequence, where stage 1 is characterized by a healthy retinal structure and function, and stage 6 by complete degeneration of photoreceptors and RPE cells with loss of function.[25] The first detectable changes were described occurring in fundus AF imaging as an increase in intensity (stage 2) and texture (the spatial variation of fundus AF intensity; stage 3). Functional decline, as surrogate for partial photoreceptor degeneration, defines stage 4. Notably, slowing of the retinoid cycle (i.e., a prolonged dark adaptation) was not present beforehand, which is in in contrast to the somewhat inconsistent observations in the *Abca4*$^{-/-}$ mouse. In stage 5, functional deficits increase together with a decline in mean AF intensity.[25] Two studies have reported that loss of 790 nm AF precedes loss of 480 nm AF,[11,37] and a model was suggested with decreasing 790 nm AF preceding similar changes on 488-nm AF imaging.

The *Abca4*$^{-/-}$ mouse model assessed herein mainly reflects the early stages of this proposed human disease sequence and may aid in adjusting suggested diseases models. There is an early diffuse increase in 488-nm fundus AF intensity due to lipofuscin accumulation, followed by an increase in texture (i.e., spatial variation of fundus AF and occurrence of fleck-like lesions). The mouse model suggests that preceding functional decline (as observed in 18-month-old *Abca4*$^{-/-}$ mice, equivalent to the human disease stage 4) 790-nm fundus AF increases, most likely due to formation of melanolipofuscin. Higher long-wavelength AF intensity has been observed in humans irrespective of marked textural changes[9]; however, this phenotypic feature had not been placed into the context of the disease sequence. A fleck-like increase and subsequent decrease of 790 nm AF may precede similar changes on 488 nm AF, and functional decline ensues.

Progressive loss of cones starting in stage 2 has been shown by adaptive optics SLO imaging in the posterior fundus of patients with Stargardt disease,[38] and spectral domain OCT imaging has suggested that foveal photoreceptor damage may occur before occurrence of characteristic AF patterns.[39] In the *Abca4*$^{-/-}$ mouse, functional testing using ERG and histologic analysis does not suggest significant photoreceptor loss at a similar disease stage. This discrepancy may be explained by the different anatomy of the human macula and the low number of cones in the mouse retina. The human macula with its particular anatomy and physiology appears most vulnerable to the development of functionally relevant retinal atrophy in ABCA4-related retinal disease. The mouse model, however, might rather mimic the disease course in more peripheral human retina. Also, various human mutations have different effects on disease manifestation and progression,[40] and this may differ from the null-background in the *Abca4*$^{-/-}$ mouse.

Stargardt patients have been observed to have fundus AF intensity (excitation: 510 nm; emission: 620 nm) above the age-matched 99.99% CI of healthy control subjects.[10] As in our study, there appeared to be a trend that the increase of fundus AF in Stargardt patients is more pronounced at younger age,[10,41] possibly with a ceiling effect later in life, while there

appears to be a quasi linear increase with age in healthy controls. The observed approximate 2-fold increase of AF intensity compared with WT mice is in line with the data by Delori et al.[10] in Stargardt patients. Normal or decreased fundus AF levels in patients with Stargardt diseases as reported by Lois et al.[42] might be due to assessment at various disease stages (see above), or may be explained by different mutational effects, gene–gene interactions, environmental modifiers, and genetic heterogeneity.

Conclusions

Progressive changes in fundus AF are observed in a large number of human retinal diseases, including AMD and most inherited retinal dystrophies, and such changes have been suggested as markers for disease progression. The use of the same in vivo imaging technique to assess animal models allows investigation of the cellular and biochemical alterations underlying changes visible on fundus AF imaging, and may, thus, further the understanding of fundus AF in human retinal disease.

We show that quantitative and qualitative changes in fundus AF can be assessed in the *Abca4*$^{-/-}$ mouse. Increased fundus AF intensity (488 nm excitation light) is related to an increase in lipofuscin and one of its major constituents, A2E, and may therefore be used as a surrogate marker for monitoring efficacy of drug or gene therapy treatments aimed at lowering RPE-lipofuscin. Using similar imaging techniques in patients, results from preclinical studies may be directly translated into clinical trials. Of note, increased lipofuscin-associated AF alone did not result in functional decline. However, quantitation of 790 nm AF may be a useful early marker for functionally relevant RPE alteration. Increased 790 nm AF follows lipofuscin accumulation, is associated with changes in the melanosome compartment and might precede functionally relevant cell loss.

Note after acceptance of the manuscript: During the review of this manuscript, a paper with partly similar content was published by Sparrow et al.[43] in the same journal. A discussion relating to their findings can be found in the Supplementary Material.

Acknowledgments

The authors thank Sylvia Bolz for her excellent technical assistance (Section of Experimental Vitreoretinal Surgery; Centre of Ophthalmology, Institute for Ophthalmic Research, Tübingen, Germany).

Supported by The European Commission, FP7, Marie Curie Intra-European Fellowship 237238; ProRetina; Fight for Sight; Wellcome Trust Grant 086868/Z/08/Z; Health Foundation; Royal College of Surgeons of Edinburgh; and National Institute for Health Research Oxford and Moorfields Biomedical Research Centres.

Disclosure: **P. Charbel Issa**, None; **A.R. Barnard**, None; **M.S. Singh**, None; **E. Carter**, None; **Z. Jiang**, None; **R.A. Radu**, None; **U. Schraermeyer**, None; **R.E. MacLaren**, None

References

1. Allikmets R, Singh N, Sun H, et al. A photoreceptor cell-specific ATP-binding transporter gene (ABCR) is mutated in recessive Stargardt macular dystrophy. *Nat Genet*. 1997;15:236–246.
2. Cremers FP, van de Pol DJ, van Driel M, et al. Autosomal recessive retinitis pigmentosa and cone-rod dystrophy caused by splice site mutations in the Stargardt's disease gene ABCR. *Hum Mol Genet*. 1998;7:355–362.
3. Martinez MA, Paloma E, Allikmets R, et al. Retinitis pigmentosa caused by a homozygous mutation in the Stargardt disease gene ABCR. *Nat Genet*. 1998;18:11–12.
4. Maugeri A, Klevering BJ, Rohrschneider K, et al. Mutations in the ABCA4 (ABCR) gene are the major cause of autosomal recessive cone-rod dystrophy. *Am J Hum Genet*. 2000;67:960–966.
5. Klevering BJ, Deutman AF, Maugeri A, Cremers FP, Hoyng CB. The spectrum of retinal phenotypes caused by mutations in the ABCA4 gene. *Graefes Arch Clin Exp Ophthalmol*. 2005;243:90–100.
6. Allikmets R, Shroyer NF, Singh N, et al. Mutation of the Stargardt disease gene (ABCR) in age-related macular degeneration. *Science*. 1997;277:1805–1807.
7. Poloschek CM, Bach M, Lagreze WA, et al. ABCA4 and ROM1: implications for modification of the PRPH2-associated macular dystrophy phenotype. *Invest Ophthalmol Vis Sci*. 2010;51:4253–4265.
8. Stargardt K. Über familiäre, progressive Degenerationen in der Maculagegend des Auges. *Graefes Arch Clin Exp Ophthalmol*. 1909;71:534–550.
9. Cideciyan AV, Swider M, Aleman TS, et al. Reduced-illuminance autofluorescence imaging in ABCA4-associated retinal degenerations. *J Opt Soc Am A Opt Image Sci Vis*. 2007;24:1457–1467.
10. Delori FC, Staurenghi G, Arend O, Dorey CK, Goger DG, Weiter JJ. In vivo measurement of lipofuscin in Stargardt's disease–Fundus flavimaculatus. *Invest Ophthalmol Vis Sci*. 1995;36:2327–2331.
11. Cukras CA, Wong WT, Caruso R, Cunningham D, Zein W, Sieving PA. Centrifugal expansion of fundus autofluorescence patterns in Stargardt disease over time. *Arch Ophthalmol*. 2012;130:171–179.
12. Weng J, Mata NL, Azarian SM, Tzekov RT, Birch DG, Travis GH. Insights into the function of Rim protein in photoreceptors and etiology of Stargardt's disease from the phenotype in abcr knockout mice. *Cell*. 1999;98:13–23.
13. Schütt F, Davies S, Kopitz J, Holz FG, Boulton ME. Photodamage to human RPE cells by A2-E, a retinoid component of lipofuscin. *Invest Ophthalmol Vis Sci*. 2000;41:2303–2308.
14. Sparrow JR, Nakanishi K, Parish CA. The lipofuscin fluorophore A2E mediates blue light-induced damage to retinal pigmented epithelial cells. *Invest Ophthalmol Vis Sci*. 2000;41:1981–1989.
15. Bergmann M, Schütt F, Holz FG, Kopitz J. Inhibition of the ATP-driven proton pump in RPE lysosomes by the major lipofuscin fluorophore A2-E may contribute to the pathogenesis of age-related macular degeneration. *FASEB J*. 2004;18:562–564.
16. Holz FG, Schütt F, Kopitz J, et al. Inhibition of lysosomal degradative functions in RPE cells by a retinoid component of lipofuscin. *Invest Ophthalmol Vis Sci*. 1999;40:737–743.
17. Zhou J, Jang YP, Kim SR, Sparrow JR. Complement activation by photooxidation products of A2E, a lipofuscin constituent of the retinal pigment epithelium. *Proc Natl Acad Sci U S A*. 2006;103:16182–16187.
18. Grey AC, Crouch RK, Koutalos Y, Schey KL, Ablonczy Z. Spatial localization of A2E in the retinal pigment epithelium. *Invest Ophthalmol Vis Sci*. 2011;52:3926–3933.
19. Radu RA, Han Y, Bui TV, et al. Reductions in serum vitamin A arrest accumulation of toxic retinal fluorophores: a potential therapy for treatment of lipofuscin-based retinal diseases. *Invest Ophthalmol Vis Sci*. 2005;46:4393–4401.
20. Radu RA, Yuan Q, Hu J, et al. Accelerated accumulation of lipofuscin pigments in the RPE of a mouse model for ABCA4-mediated retinal dystrophies following vitamin A supplementation. *Invest Ophthalmol Vis Sci*. 2008;49:3821–3829.
21. Charbel Issa P, Singh MS, Lipinski DM, et al. Optimization of in vivo confocal autofluorescence imaging of the ocular fundus in mice and its application to models of human retinal degeneration. *Invest Ophthalmol Vis Sci*. 2012;53:1066–1075.

Investigative Ophthalmology & Visual Science

22. Radu RA, Hu J, Yuan Q, et al. Complement system dysregulation and inflammation in the retinal pigment epithelium of a mouse model for Stargardt macular degeneration. *J Biol Chem*. 2011;286:18593–18601.
23. Moiseyev G, Nikolaeva O, Chen Y, Farjo K, Takahashi Y, Ma JX. Inhibition of the visual cycle by A2E through direct interaction with RPE65 and implications in Stargardt disease. *Proc Natl Acad Sci U S A*. 2010;107:17551–17556.
24. Delori FC, Dorey CK, Staurenghi G, Arend O, Goger DG, Weiter JJ. In vivo fluorescence of the ocular fundus exhibits retinal pigment epithelium lipofuscin characteristics. *Invest Ophthalmol Vis Sci*. 1995;36:718–729.
25. Cideciyan AV, Aleman TS, Swider M, et al. Mutations in ABCA4 result in accumulation of lipofuscin before slowing of the retinoid cycle: a reappraisal of the human disease sequence. *Hum Mol Genet*. 2004;13:525–534.
26. Boyer NP, Higbee D, Currin MB, et al. Lipofuscin and N-retinylidene-N-retinylethanolamine (A2E) accumulate in retinal pigment epithelium in absence of light exposure: their origin is 11-cis-retinal. *J Biol Chem*. 2012;287:22276–22286.
27. Delori F, Greenberg JP, Fischer J, et al. Quantitative measurements of autofluorescence with the scanning laser ophthalmoscope. *Invest Ophthalmol Vis Sci*. 2011;52:9379–9390.
28. Keilhauer CN, Delori FC. Near-infrared autofluorescence imaging of the fundus: visualization of ocular melanin. *Invest Ophthalmol Vis Sci*. 2006;47:3556–3564.
29. Kayatz P, Thumann G, Luther TT, et al. Oxidation causes melanin fluorescence. *Invest Ophthalmol Vis Sci*. 2001;42:241–246.
30. Sarna T, Burke JM, Korytowski W, et al. Loss of melanin from human RPE with aging: possible role of melanin photooxidation. *Exp Eye Res*. 2003;76:89–98.
31. Wu L, Nagasaki T, Sparrow JR. Photoreceptor cell degeneration in Abcr (–/–) mice. *Adv Exp Med Biol*. 2010;664:533–539.
32. Rozanowski B, Burke JM, Boulton ME, Sarna T, Rozanowska M. Human RPE melanosomes protect from photosensitized and iron-mediated oxidation but become pro-oxidant in the presence of iron upon photodegradation. *Invest Ophthalmol Vis Sci*. 2008;49:2838–2847.
33. Pawar AS, Qtaishat NM, Little DM, Pepperberg DR. Recovery of rod photoresponses in ABCR-deficient mice. *Invest Ophthalmol Vis Sci*. 2008;49:2743–2755.
34. Allocca M, Doria M, Petrillo M, et al. Serotype-dependent packaging of large genes in adeno-associated viral vectors results in effective gene delivery in mice. *J Clin Invest*. 2008;118:1955–1964.
35. Han Z, Conley SM, Makkia RS, Cooper MJ, Naash MI. DNA nanoparticle-mediated ABCA4 delivery rescues Stargardt dystrophy in mice. *J Clin Invest*. 2012;122:3221–3226.
36. Kong J, Kim SR, Binley K, et al. Correction of the disease phenotype in the mouse model of Stargardt disease by lentiviral gene therapy. *Gene Therapy*. 2008;15:1311–1320.
37. Kellner S, Kellner U, Weber BH, Fiebig B, Weinitz S, Ruether K. Lipofuscin- and melanin-related fundus autofluorescence in patients with ABCA4-associated retinal dystrophies. *Am J Ophthalmol*. 2009;147:895–902. 902 e891.
38. Chen Y, Ratnam K, Sundquist SM, et al. Cone photoreceptor abnormalities correlate with vision loss in patients with Stargardt disease. *Invest Ophthalmol Vis Sci*. 2011;52:3281–3292.
39. Gomes NL, Greenstein VC, Carlson JN, et al. A comparison of fundus autofluorescence and retinal structure in patients with Stargardt disease. *Invest Ophthalmol Vis Sci*. 2009;50:3953–3959.
40. Cideciyan AV, Swider M, Aleman TS, et al. ABCA4 disease progression and a proposed strategy for gene therapy. *Hum Mol Genet*. 2009;18:931–941.
41. von Rückmann A, Fitzke FW, Bird AC. In vivo fundus autofluorescence in macular dystrophies. *Arch Ophthalmol*. 1997;115:609–615.
42. Lois N, Halfyard AS, Bird AC, Holder GE, Fitzke FW. Fundus autofluorescence in Stargardt macular dystrophy-fundus flavimaculatus. *Am J Ophthalmol*. 2004;138:55–63.
43. Sparrow JR, Blonska A, Flynn E, et al. Quantitative fundus autofluorescence in mice: correlation with HPLC quantitation of RPE lipofuscin and measurement of retina outer nuclear layer thickness. *Invest Ophthalmol Vis Sci*. 2013;54:2812–2820.

Investigative Ophthalmology & Visual Science